Unstable periodic orbits and the dimensions of multifractal chaotic attractors

Celso Grebogi
Laboratory for Plasma and Fusion Energy Studies, University of Maryland, College Park, Maryland 20742

Edward Ott
Laboratory for Plasma and Fusion Energy Studies, University of Maryland, College Park, Maryland 20742
and Department of Electrical Engineering and Department of Physics, University of Maryland, College Park, Maryland 20742

James A. Yorke
Institute for Physical Science and Technology and Department of Mathematics, University of Maryland, College Park, Maryland 20742

(Received 28 September 1987)

The probability measure generated by typical chaotic orbits of a dynamical system can have an arbitrarily fine-scaled interwoven structure of points with different singularity scalings. Recent work has characterized such measures via a spectrum of fractal dimension values. In this paper we pursue the idea that the infinite number of unstable periodic orbits embedded in the support of the measure provides the key to an understanding of the structure of the subsets with different singularity scalings. In particular, a formulation relating the spectrum of dimensions to unstable periodic orbits is presented for hyperbolic maps of arbitrary dimensionality. Both chaotic attractors and chaotic repellers are considered.

I. INTRODUCTION

The long time distribution generated by a typical orbit of a chaotic nonconservative dynamical system is generally highly singular. The subset of phase space to which the orbit asymptotes with time, the attractor, can be geometrically fractal. Furthermore, the distribution of orbit points on the attractor can have an arbitrarily fine-scaled interwoven structure of hot and cold spots. Sets with such distributions have been called *multifractals. By hot and cold spots we mean points on* the attractor for which the frequency of close approach of typical orbits is either much greater than typical (a hot spot) or much less than typical (a cold spot). Recently there has been much work developing ways of quantitatively characterizing how such chaotic orbits distribute themselves on attractors.[1-4] In particular, the spectrum of fractal dimensions introduced in Refs. 2-4 are sensitive to the characteristics of the structure of hot and cold spots on the attractor. In this paper we present results which show that, for a large class of chaotic attractors, the infinite number of unstable periodic orbits embedded in the attractor provide the key to an understanding of such issues. (A brief preliminary report of some of this work appears in Grebogi, Ott, and Yorke.[5])

The importance of unstable periodic orbits in determining ergodic properties of chaotic systems has long been recognized in the mathematical literature (e.g., Bowen[6] and Katok[7]). For some more recent work see Refs. 8 and 9 which also illustrate the important point that information about unstable periodic orbits is readily accessible from numerical computation (and perhaps experimentally[9,10]) and can be used for determining ergodic properties. In addition, in the theory of quantum chaos, the distribution of energy levels can be related to unstable periodic orbits of the classical Hamiltonian.[11-13] Another case where unstable periodic orbits appear[10] is in determining the behavior near parameter values where sudden changes in chaotic attractors occur [the argument in connection with our Fig. 1 is similar to that for Eq. (2) of Ref. 10].

The organization of this paper is as follows. Section II presents a discussion of the pointwise dimension for attractors and shows that hot and cold spots occur on the unstable manifolds of saddle periodic orbits in the attractor. Numerical experiments illustrating this are also presented. Section III reviews recent work on the dimensions of attractors including the partition function formalism.[4] Section IV presents our results relating the distribution of typical chaotic orbits on attractors and the associated fractal dimensions to the unstable periodic orbits. Section V illustrates the material of Sec. IV with examples. Arguments yielding the results stated in Sec. IV are presented in Sec. VI for the case of hyperbolic attractors. Section VII treats the case of chaotic sets which are repelling rather than attracting.

The dynamical systems to be discussed throughout this paper are d-dimensional maps of the form $\underline{x}_{n+1}=\underline{F}(\underline{x}_n)$, where $\underline{x}$ is a vector in the d-dimensional phase space of the system. An *attractor* A for such a system is a closed set, invariant under $\underline{F}$, which is the limit set as time goes to $+\infty$ for almost every initial condition in some neighborhood of A. (By "almost every" we mean that the set of initial conditions in the neighborhood that do not approach A can be covered by a set of d-dimensional cubes of arbitrarily small total volume.) The *basin of attraction* for the attractor is the closure of the set of points which asymptote to the attractor as time goes to $+\infty$. In the

case of continuous time systems (flows), we can think of $\underline{F}(\underline{x})$ as arising from a Poincaré surface of section.

II. POINTWISE DIMENSION

For most purposes we may think of the *natural measure* of an attractor as follows: For a subset S of the phase space and an initial condition $\underline{x}$ in the basin of attraction of the attractor, we define $\mu(\underline{x},S)$ as the fraction of time the trajectory originating at $\underline{x}$ spends in S in the limit that the length of the trajectory goes to infinity. If $\mu(\underline{x},S)$ is the same for almost every $\underline{x}$ in the basin of attraction, then we denote this value $\mu(S)$ and say that μ is the natural measure of the attractor (cf. Appendix). Henceforth, we assume that the attractor has a natural measure. In particular, this means that the attractor is ergodic (i.e., it cannot be split into two disjoint pieces that each have positive natural measure and are invariant under application of $\underline{F}$).

Let $B(l,\underline{x})$ denote a d-dimensional ball of radius l centered at a point $\underline{x}$ on an attractor embedded in the d-dimensional phase space of the dynamical system being considered. Then the pointwise dimension (at the point $\underline{x}$) of the attractor is defined as

$$D_p(\underline{x})=\lim_{l\to 0}\frac{\log\mu(B(l,\underline{x}))}{\log l} \tag{2.1}$$

or $\mu(B(l,\underline{x}))\sim l^{D_p(\underline{x})}$. For *almost every* point with respect to the natural measure on the attractor, $D_p(\underline{x})$ takes on a common value and is equal to the information dimension (defined in Sec. III). That is, the set of points on the chaotic attractor for which $D_p(\underline{x})$ is not this common value may be covered with a set of d-dimensional cubes of varying sizes which together contain an arbitrarily small amount of the natural measure of the attractor. [Points $\underline{x}$ where $D_p(\underline{x})$ is greater than (less than) the common value it assumes at almost every point with respect to the natural measure are the hot (cold) spots referred to in Sec. I.] For example, a chaotic attractor typically has a dense set of unstable periodic orbits embedded within it, and, as we shall see, $D_p(\underline{x})$ with $\underline{x}$ on one of these periodic orbits does not take on the typical values. The periodic points, however, are countable and so have zero measure. Nevertheless, it is a main point of this paper that this zero measure set is important and leads to interesting properties of the attractor.

To see why $D_p(\underline{x})$ is the same for almost every $\underline{x}$ with respect to the natural measure, assume that it is not. Then we can pick some D_{p0} such that there is a nonzero amount for the natural measure of the attractor for which $D_p(\underline{x})>D_{p0}$ and another nonzero amount for which $D_p(\underline{x})\le D_{p0}$. Thus the attractor is divided into two disjoint sets, $A_>$ and $A_<$, $\mu(A_>)+\mu(A_<)=1$, $\mu(A_\gtrless)>0$. From the definition (2.1), one can show that $D_p(\underline{x})$ is invariant to smooth changes of coordinates. In particular, for a smooth map $\underline{x}_{n+1}=\underline{F}(\underline{x}_n)$, we can take $\underline{y}=\underline{F}(\underline{x})$ as the change of coordinates. It follows that $D_p(\underline{x})=D_p(\underline{F}(\underline{x}))$. Thus the sets $A_>$ and $A_<$ are invariant under $\underline{F}$. This implies that every orbit on the attractor is confined either to $A_>$ or $A_<$. Hence, contrary to our assumption that the attractor has a natural measure, the attractor has been decomposed into two disjoint $\underline{F}$ invariant sets. We conclude that $D_p(\underline{x})$ must be the same for almost every $\underline{x}$ with respect to the natural measure on the attractor.

Returning now to consideration of the zero measure set of points $\underline{x}$ for which $D_p(\underline{x})$ is not typical (i.e., is not the common value assumed at almost every $\underline{x}$ on the attractor) and taking the map to be two dimensional ($d=2$), we will obtain the following result. Let j be an index labeling the fixed points of the n times iterated map $\underline{F}^n$. (The components of a period n orbit are fixed points of $\underline{F}^n$.) We assume that the Jacobian matrix of $\underline{F}^n$ at fixed point j has one unstable direction and one stable direction. Then for any point $\underline{x}$ *on the unstable manifold* of fixed point j of $\underline{F}^n$,

$$D_p(\underline{x})=1-\frac{\log\lambda_{1j}}{\log\lambda_{2j}}\ , \tag{2.2}$$

where $\lambda_{1j}>1$ and $\lambda_{2j}<1$ are the magnitudes of the unstable and stable eigenvalues of the Jacobian matrix of $\underline{F}^n$. Since points on different periodic orbits typically have different eigenvalues, $D_p(\underline{x})$ will clearly be different for different periodic orbits and hence will not be the typical $D_p(\underline{x})$.

To obtain (2.2) consider a point $\underline{x}_0$ on the unstable manifold of a saddle periodic point and two small circular disks centered at $\underline{x}_0$ with radii l_1 and l_2, where $l_1/l_2=\lambda_{2j}^{-1}$. We iterate the two disks backward a large integral number of periods so that the two disks are now similar ellipses close to the saddle and with their major axes parallel to the stable manifold of the saddle (cf. Fig. 1). We now iterate the l_2 ellipse backward one more period. Since it is close to the saddle, its backward iteration by one period is governed by the linearized map at the saddle (i.e., by the eigenvalues λ_{1j} and λ_{2j}). Thus, since we choose $l_1/l_2=\lambda_{2j}^{-1}$, the major diameter of the l_2 ellipse is now the same as that for the l_1 ellipse, while its minor diameter is smaller than that for the l_1 ellipse by the factor $\lambda_{2j}/\lambda_{1j}$. The inverse images of the disks contain the same natural measure as the original disks. Thus, treating the attractor measure as if it were smooth along the unstable direction, we have $\mu(B(l_2,\underline{x}_0))/\mu(B(l_1,\underline{x}_0))=\lambda_{2j}/\lambda_{1j}$. Setting $\mu(B(l,\underline{x}_0))\sim l^{D_P}$ and $l_2=l_1\lambda_{2j}$, this yields Eq. (2.2), the desired result.

We have tested Eq. (2.2) numerically using the Henon map given by

$$\begin{aligned} x_{n+1}&=1.42-x_n^2+0.3y_n\ ,\\ y_{n+1}&=x_{n+1}\ . \end{aligned} \tag{2.3}$$

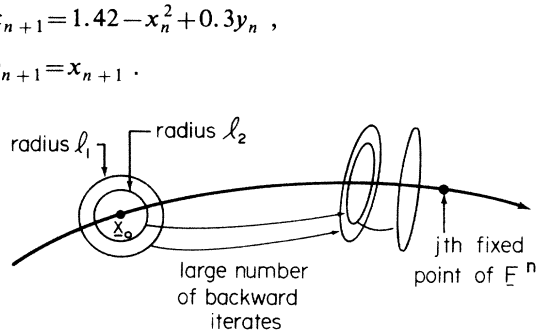

FIG. 1. Schematic for the derivation of Eq. (2.2).

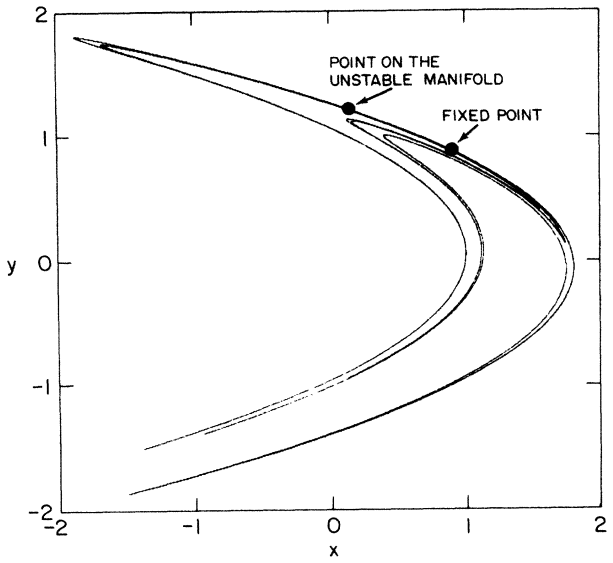

FIG. 2. Plot of the iterates of the Henon map (2.3).

In Fig. 2, we plot iterates of the map (2.3) to show the attractor. In this figure we also indicate the location of a point which we have accurately determined to be on the unstable manifold of an unstable fixed point (i.e., a period one unstable orbit) of the map (2.3). In Fig. 3, we display the result of a calculation of the pointwise dimension $D_p(\underline{x})$ for $\underline{x}$ at this point. In this figure, we plot $\mu(B(l,\underline{x}))$ versus l on a log-log scale. Here $\mu(B(l,\underline{x}))$ is obtained by iterating a randomly chosen initial condition in the basin of the attractor 10^6 times (so that the orbit is essentially on the attractor) and then determining the fraction of subsequent orbit points which fall in $B(l,\underline{x})$ on further iteration. The numerically determined pointwise dimension is the slope of the straight line through the points in Fig. 3; we obtain $D_p(\underline{x}) \cong 1.36$. The magnitudes of the eigenvalues at the fixed point are $1.94\cdots$ and $0.155\cdots$, which, when inserted in Eq. (2.2), yield $D_p(\underline{x}) = 1.36$, in agreement with the data in Fig. 3.

Next we obtain a typical point $\underline{x}$ on the attractor which is within a small distance (1.5×10^{-4} in this case) of the previously chosen point on the unstable manifold of the fixed point. We do this by randomly picking an initial condition, preiterating 2×10^6 times, and then iterating the map until the orbit falls within a circle of radius 2×10^{-4} centered at the previously obtained point on the unstable manifold. Results for $\mu(B(l,\underline{x}))$ versus l for this point are shown in Fig. 4. For $l > 1.5\times 10^{-4}$ the slope of the straight line fitted to the numerical data is 1.36, which is the same value as obtained in Fig. 3 for the point on the unstable manifold. This agreement is as expected, since for $l \gg 10^{-4}$, the two points are essentially indistinguishable. However, for data points in the range $6\times 10^{-6} < l < 1.5\times 10^{-4}$, we find that the slope of a fitted line is 1.21, which is significantly different from the 1.36 slope for $l > 1.5\times 10^{-4}$.

There are an infinite number of unstable periodic orbits on the attractor. Thus, although it is true that all typical $\underline{x}$ must have a common value for $D_p(\underline{x})$, one might suspect that there will be significant fluctuations in numerically determined values of D_p, since such calculations are necessarily restricted to a finite range of l. This seems to be the case: We have numerically determined $D_p(\underline{x})$ for the map (2.3) using a range $10^{-1} \leq l \leq 10^{-5}$ at 20 different typical points, and we find considerable variation in the resulting numerically determined pointwise dimensions. A list of the 20 values obtained appears in Table I. In obtaining these values, a least square fit was used in $10^{-1} \leq l \leq 1.22\times 10^{-5}$, and the root-mean-square deviation of the least square fit is also shown in Table I. This root-mean-square deviation of the fit for $D_p(\underline{x})$ at individual $\underline{x}$ values is small compared with the standard deviation (0.10) about the mean (1.27) obtained by using the twenty $D_p(\underline{x})$ values (given in the first column of Table I). (The 20 typical $\underline{x}$ values used were obtained by choosing a random initial condition in the basin of the attractor, iterating it 20×10^6 times, and selecting every millionth iterate.)

The Kaplan-Yorke formula, discussed in Sec. IV, predicts the typical value of the pointwise dimension in terms of the Lyapunov numbers. For the case considered here, the predicted value is 1.26, which is in good agreement with our mean of the twenty numerically obtained D_p values but is far from the value obtained in Fig. 3.

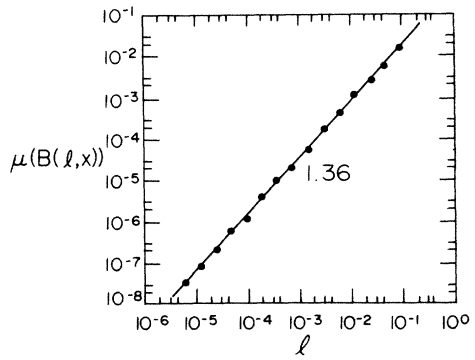

FIG. 3. Log-log plot of $\mu(B(l,x))$ vs l for a point on the unstable manifold of the fixed point.

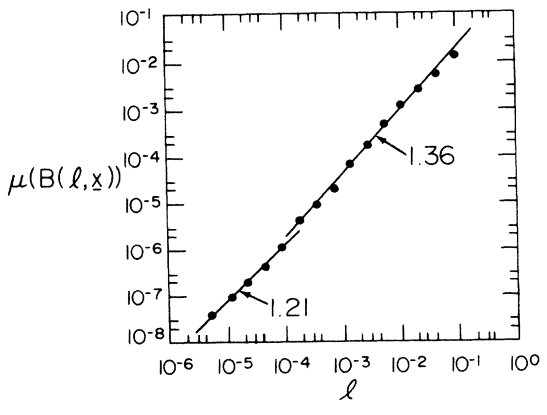

FIG. 4. Log-log plot of $\mu(B(l,\underline{x}))$ vs l for a typical point on the attractor which is within 1.5×10^{-4} of the point on the unstable manifold of the fixed point.

TABLE I. Result of pointwise dimension calculations for 20 typical points. Mean equals 1.27±0.10

$D_p(\underline{x})$	rms deviation of fit
1.29	0.03
1.31	0.03
1.12	0.02
1.34	0.03
1.21	0.02
1.25	0.02
1.21	0.04
1.34	0.03
1.31	0.04
1.38	0.02
1.25	0.04
1.28	0.03
1.26	0.03
1.34	0.03
1.33	0.03
1.15	0.02
1.02	0.01
1.32	0.03
1.41	0.02
1.37	0.02

III. DIMENSIONS OF MULTIFRACTAL CHAOTIC ATTRACTORS

In this section we review past work on the dimensions characterizing multifractal chaotic attractors.[2-4] References 2 and 3 consider the quantity $\tilde{D}_q$ defined by

$$\tilde{D}_q = \frac{1}{q-1} \lim_{l \to 0} \frac{\log \sum_{i=1}^{N(l)} p_i^q}{\log l} , \tag{3.1}$$

where the attractor is covered with $N(l)$ d-dimensional cubes from a grid of unit length l, and p_i is the natural measure of the attractor in the ith cube. Taking the limit $q \to 1$, Eq. (3.1) yields[2,3]

$$\tilde{D}_1 = \lim_{l \to 0} \left[\sum_i p_i \log p_i \right] \Big/ \log l , \tag{3.2}$$

which is called the information dimension of the attractor. It is $\tilde{D}_1$ which is the common value assumed by $D_p(\underline{x})$ for almost all $\underline{x}$ with respect to the natural measure on the attractor.[1] We may think of the information dimension as the capacity dimension (cf. below) of the smallest set which contains most of the natural measure of the attractor.[1]

As q is increased past 1, the contribution of the sum $\sum_i p_i^q$ from a relatively few boxes with very little of the total attractor measure but with larger p_i than typical (i.e., hot spots) becomes relatively more important. Similarly, as q is decreased from one, the contribution from low probability boxes begins to be more important. For example, for $q=0$, Eq. (3.1) yields

$$\tilde{D}_0 = -\lim_{l \to 0} \log N(l) / \log l , \tag{3.3}$$

which is known as the capacity or box-counting dimension of the attractor. Note that all boxes on the attractor contribute democratically to (3.3) no matter what their natural measure p_i is. For typical chaotic attractors, it is to be expected that $\tilde{D}_0 > \tilde{D}_1$, since low-probability boxes (cold regions) containing very little of the total natural measure on the attractor may be vastly more numerous than those required to cover most of the natural measure on the attractor.[1]

At this point it is appropriate to discuss another definition of dimension, the Hausdorff dimension,[14] which is, in fact, an older concept than either the capacity[15] or information dimensions.[16] To define the Hausdorff dimension, we cover the attractor with d-dimensional cubes of variable edge length l_i, all of which we restrict to be no bigger than some value l ($l_i \le l$). We then form the quantity

$$\Gamma_H(D,l,\{l_i\}) = \sum_i l_i^D . \tag{3.4}$$

Next the covering of cubes is optimized so as to make the sum $\sum l_i^D$, minimum,

$$\Gamma_H(D,l) = \inf_{\{l_i\}} \sum_i l_i^D , \tag{3.5}$$

where the infimum is taken over all possible collections of cubes that cover the attractor subject to the constraint $l_i \le l$. Finally, the limit $l \to 0$ is taken,

$$\Gamma_H(D) = \lim_{l \to 0} \Gamma_H(D,l) . \tag{3.6}$$

The quantity $\Gamma_H(D)$ can be shown to be either zero or infinity except at a critical value of D [cf. Fig. 5(a)]. This critical value defines the Hausdorff dimension which we denote D_H.

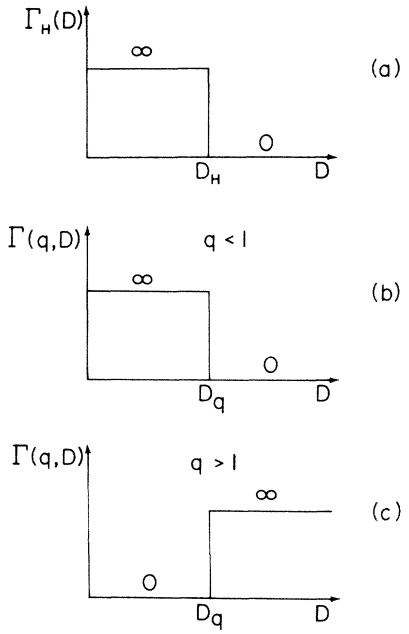

FIG. 5. (a) $\Gamma_H(D)$ vs D_H. (b) $\Gamma(q,D)$ for $q<1$. (c) $\Gamma(q,D)$ for $q>1$.

The capacity dimension $\tilde{D}_0$ and the Hausdorff dimension are closely related. In particular, if we do not optimize over the cube covering, but instead use a cubic grid covering of fixed length l, then all the l_i in (3.4) are equal to l, and we have $\Gamma_H^{(\text{grid})}(D,l)=N(l)l^D$. Equation (3.3) is satisfied by $N(l)\sim l^{-\tilde{D}_0}$, which yields $\Gamma_H^{(\text{grid})}(D,l)\sim l^{D-\tilde{D}_0}$. In the limit $l\to 0$, $\Gamma_H^{(\text{grid})}$ is zero or infinity [as in Fig. 5(a)] with the transition at $D=\tilde{D}_0$. Since the covering using a cubic grid may not be optimal, $\Gamma_H^{(\text{grid})}(D,l)\geq\Gamma_H(D,l)$ and

$$\tilde{D}_0\geq D_H \ .$$

For examples of ergodic chaotic attractors, where $\tilde{D}_0$ and D_H are analytically calculable, it is found[1] that $\tilde{D}_0=D_H$, and it has been conjectured that this is to be expected, in general, for typical ergodic chaotic attractors (although it is easy to construct sets[1] which are not attractors which have $\tilde{D}_0>D_H$).

Reference 4 gives a formalism which essentially generalizes the Hausdorff procedure and its relation to $\tilde{D}_0$ so that $\tilde{D}_q$ for arbitrary q is treated. In particular, again say we cover the attractor with cubes of variable edge length l_i, but now consider the following quantity, which in analogy with statistical mechanics, has been called the partition function,

$$\Gamma(q,D,l,\{l_i\})=\sum_i p_i^q/l_i^\tau, \quad \tau=(q-1)D \tag{3.7}$$

where $D\geq 0$. Optimize over covering $\{l_i\}$,

$$\Gamma(q,D,l)=\begin{cases}\sup[\Gamma(q,D,l,\{l_i\})] & \text{for } q>1 \ , \\ \inf[\Gamma(q,D,l,\{l_i\})] & \text{for } q<1 \ ,\end{cases} \tag{3.8}$$

and take the limit $l\to 0$,

$$\Gamma(q,D)=\lim_{l\to 0}\Gamma(q,D,l) \ . \tag{3.9}$$

Again $\Gamma(q,D)$ is zero or infinity. The transition point for $\Gamma(q,D)$ is denoted D_q. [$\Gamma(q,D)=0$ for $(q-1)D<(q-1)D_q$, and $\Gamma(q,D)=\infty$ for $(q-1)D>(q-1)D_q$ (cf. Figs. 5(b) and 5(c)).]

Again say that we do not optimize over coverings, but instead use a cubic grid, of basic length l, then $l_i=l$ and we have $\sum_i p_i^q/l_i^\tau=l^{-\tau}\sum_i p_i^q$. From Eq. (3.1), $\sum_i p_i^q\sim l^{(q-1)\tilde{D}_q}$ and hence $\sum_i p_i^q/l_i^\tau\sim l^{(q-1)(\tilde{D}_q-D)}$, which,in the limit $l\to 0$, pass from 0 to ∞ at $D=\tilde{D}_q$. Since in this the optimization over coverings, prescribed in Eq. (3.8), is not done, the quantity D_q defined by Eqs. (3.7)–(3.9) is necessarily less than or equal to $\tilde{D}_q$,

$$D_q\leq\tilde{D}_q \ . \tag{3.10}$$

However, as for the Hausdorff and capacity dimensions, it is to be expected that, in practice, the equality in (3.10) typically holds for chaotic attractors.

A central result of Halsey *et al.*[4] was the demonstration of the way in which D_q is connected to the hot and cold points on the attractor (i.e., those points $\underline{x}$ on the attractor for which the pointwise dimension $(D_p(\underline{x})\neq\tilde{D}_1)$. In particular, they consider the set of $\underline{x}$ values such that $D_p(\underline{x})=\alpha$, and they denote the Hausdorff dimension of this set by $f(\alpha)$. They show that the D_q can be explicitly obtained from the dimensions $f(\alpha)$ via the formulas,

$$df(\alpha)/d\alpha=q \ , \tag{3.11a}$$

$$(q-1)D_q=[q\alpha(q)-f(\alpha(q))] \ . \tag{3.11b}$$

IV. UNSTABLE PERIODIC ORBITS

In this section we state and discuss results obtained in Sec. VI on the relation of unstable periodic orbits on chaotic attractors to the ergodic properties of these attractors. The results to be quoted are for the case of chaotic attractors that are *mixing* and *hyperbolic*. By mixing we mean that for any two sets S_a and S_b in the phase space of the system, we have

$$\lim_{n\to\infty}\mu[S_a\cap\underline{F}^n(S_b)]=\mu(S_a)\mu(S_b) \ ,$$

where μ is the natural measure of the attractor. A chaotic attractor would not be mixing in the commonly encountered situation where the attractor consists of a finite number h of disjoint pieces, and the orbit cycles from piece to piece. In this case, instead of the map $\underline{F}$ one can consider the map $\underline{F}^h$. For $\underline{F}^h$ each of the h pieces of the attractor for $\underline{F}$ is a separate attractor in its own right and is typically mixing. Our result would then apply to the attractors of $\underline{F}^h$. Henceforth, we assume that the attractor is mixing. Hyperbolic attractors are defined in Sec. VI.

We consider a d-dimensional twice differentiable map, $\underline{x}_{m+1}=\underline{F}(\underline{x}_m)$. The magnitudes of the eigenvalues of the Jacobian matrix of the n times iterated map $\underline{F}^n$ at the jth fixed point of $\underline{F}^n$ are denoted $\lambda_{1j},\lambda_{2j},\ldots,\lambda_{uj},\lambda_{(u+1)j},\ldots,\lambda_{dj}$, where we order the eigenvalues as follows: $\lambda_{1j}\geq\lambda_{2j}\geq\cdots\geq\lambda_{uj}>1\geq\lambda_{(u+1)j}\geq\cdots\geq\lambda_{dj}$. Thus in this notation, the number of unstable eigenvalues is u. Let L_j be the product of the unstable eigenvalues at the jth fixed point of $\underline{F}^n$,

$$L_j=\lambda_{1j}\lambda_{2j}\cdots\lambda_{uj} \ . \tag{4.1}$$

Then, as shown in Sec. VI for mixing hyperbolic (axiom A) attractors, the natural probability measure of the attractor contained in some closed subset S of the d-dimensional phase space is the limit as $n\to\infty$ of the sum of the L_j^{-1} over all the fixed points j of $\underline{F}^n$ which lie in S,

$$\mu(S)=\lim_{n\to\infty}\left[\sum_{\substack{\text{fixed points}\\ \text{in } S}} L_j^{-1}\right] . \tag{4.2}$$

Thus (4.2) is essentially a representation of the natural measure in terms of the unstable periodic orbits on the attractor. In particular, in the special case where S covers the entire attractor, we have $\mu(S)=1$, and, hence, we obtain a relation amongst the unstable eigenvalues,

$$1=\lim_{n\to\infty}\sum_j L_j^{-1} \ , \tag{4.3}$$

where the sum is over all fixed points of $\underline{F}^n$ on the attractor. Equation (4.3) has been conjectured to apply in general for Hamiltonian chaotic systems[12] and has been used to derive an interesting correspondence between the ei-

genvalues of a random matrix and the statistics of the semiclassical limit of the energy levels of a bound, time-independent, quantum system whose classical limit is chaotic.[13]

We now give a partition function formulation of the multifractal properties of chaotic attractors. This formulation is in terms of the eigenvalues of the dense set of periodic saddles on the attractor [rather than in terms of the measure of coverings of the attractor, i.e., the p_i in Eqs. (3.7)]. Let

$$D \equiv \Delta + \delta \ ,$$

where Δ is the integer part of D, and $\delta \equiv D - \Delta = (D \text{ modulo } 1)$ is the fractional part of D. In addition, let

$$S_j(D) \equiv \lambda_{1j}\lambda_{2j}\cdots\lambda_{\Delta j}(\lambda_{(\Delta+1)j})^{\delta} \ . \tag{4.4}$$

[Note that $S_j(D)$ is a continuous function of D.] In terms of L_j and $S_j(D)$, the result obtained in Sec. VI for the partition function is

$$\hat{\Gamma}(q,D,n) = \sum_j L_j^{-1}[S_j(D)]^{-(q-1)} \ . \tag{4.5}$$

In the two-dimensional case with $\lambda_{1j} > 1 > \lambda_{2j}$ this reduces to

$$\hat{\Gamma}(q,D,n) = \sum_j \lambda_{1j}^{-q}\lambda_{2j}^{-(D-1)(q-1)} \ , \tag{4.6}$$

which appears in Grebogi *et al.*[5] and Morita *et al.*[5] and, for the case of the Hausdorff dimension ($q=0$), in Ref. 9. Taking the limit $n \to \infty$ is analogous to taking the limit $l \to 0$ in Eq. (3.9),

$$\hat{\Gamma}(q,D) = \lim_{n\to\infty} \hat{\Gamma}(q,D,n) \ . \tag{4.7}$$

The quantity $\hat{\Gamma}(q,D)$ is zero or infinity in analogy with the quantity $\Gamma(q,D)$ in Eq. (3.9) [cf. Figs. 5(b) and 5(c)]. We denote the value of D at the transition of $\hat{\Gamma}(q,D)$ from zero to infinity by $\hat{D}_q$ and call it the periodic point dimension.

$$\hat{\Gamma}(q,D) = \begin{cases} 0 & \text{for } (q-1)D > (q-1)\hat{D}_q \\ +\infty & \text{for } (q-1)D < (q-1)\hat{D}_q \ . \end{cases}$$

In Sec. VI we show that

$$\hat{D}_q \geq D_q \ . \tag{4.8}$$

We conjecture that for typical chaotic attractors of two-dimensional maps with $\lambda_{1j} > 1 > \lambda_{2j}$

$$\hat{D}_q = D_q \ . \tag{4.9}$$

Indeed for the two-dimensional case with $\lambda_{1j} > 1 > \lambda_{2j}$, examples are worked out in Sec. V verifying that Eq. (4.9) holds. (For further discussion see Sec. VI.)

Setting $q=1$ and comparing (4.5) with (4.3) we have $\hat{\Gamma}(1,D)=1$. Formally expanding (4.5) around $q=1$ we obtain

$$\hat{\Gamma}(q,D,n) = 1 - (q-1)\sum_j \frac{\log S_j(D)}{L_j} + O[(q-1)^2] \ .$$

Letting $n \to \infty$ the coefficient of the $(q-1)$ term may be expressed using (4.4) as

$$\lim_{n\to\infty}\left[\left[\sum_j L_j^{-1}\log(\lambda_{1j}\lambda_{2j}\cdots\lambda_{\Delta j})\right] + \delta\left[\sum_j L_j^{-1}\log\lambda_{(\Delta+1)j}\right]\right] .$$

As will become evident from a correspondence with Lyapunov numbers to be discussed subsequently, the first term in large parentheses becomes positive infinite and the second term negative infinite (both sums behave like n for large n). Thus this formal expansion in $(q-1)$ indicates that the transition value $\hat{D}_1 = \Delta_1 + \delta_1$ occurs at

$$\hat{D}_1 = \Delta_1 - \lim_{n\to\infty} \frac{\sum_j L_j^{-1}\log(\lambda_{1j}\cdots\lambda_{\Delta_1 j})}{\sum_j L_j^{-1}\log(\lambda_{(\Delta_1+1)j})} \ , \tag{4.10}$$

where (to satisfy $0 \leq \delta_1 \leq 1$) we define Δ_1 as the largest integer such that $\sum_j L_j^{-1}\log(\lambda_{1j}\cdots\lambda_{\Delta_1 j})$ is positive. We now compare (4.10) with the Kaplan-Yorke conjecture.[1,17] The Kaplan-Yorke conjecture gives a formula for $\tilde{D}_1$ [defined in (3.2)] in terms of the Lyapunov numbers of typical orbits (i.e., orbits obtained for almost every choice of initial condition in the basin of the attractor). Denoting these (typical) Lyapunov numbers

$$\lambda_1 \geq \lambda_2 \geq \cdots \geq \lambda_d \ ,$$

the Kaplan-Yorke formula states that for typical systems,

$$\tilde{D}_1 = \Delta_1 - \frac{\ln(\lambda_1\lambda_2\cdots\lambda_{\Delta_1})}{\ln(\lambda_{\Delta_1+1})} \ , \tag{4.11}$$

where here Δ_1 is the largest integer such that $\lambda_1\lambda_2\cdots\lambda_{\Delta_1} > 1$. Comparing (4.11) and (4.10), see that these equations are the same if we interpret the sums over periodic orbits in (4.10) in terms of Lyapunov numbers,

$$\log\lambda_p = \lim_{n\to\infty} \frac{1}{n}\sum_j L_j^{-1}\log\lambda_{pj} \ . \tag{4.12}$$

Equation (4.12) is reasonable since our construction, to be discussed in Sec. IV A, shows that, during n iterates of the map, each orbit on the attractor stays close to some orbit of period n, and, furthermore, the natural measure of the orbits which stay close to a given period n orbit is L_j^{-1}. [This latter statement is related to Eq. (4.2).] Thus $\tilde{D}_1 = \hat{D}_1$.

The Kaplan-Yorke conjecture Eq. (4.11) has been shown to apply in a variety of examples and numerical experiments[1] (although it has not yet been proven in general). The correspondence of the $q \to 1$ limit of Eq. (4.5) [i.e., Eq. (4.10)] with the Kaplan-Yorke formula (4.11) supports our conjecture, Eq. (4.9).

Note that the two-dimensional map result for the pointwise dimension on the unstable manifolds of periodic orbits, Eq. (2.2), is the same as (4.11) with $d=2$ and the Lyapunov numbers of a typical orbit replaced by the magnitudes of the eigenvalues of the periodic orbit, $\lambda_{1j} > 1 > \lambda_{2j}$. A generalization of Eq. (2.2) to d-dimensional maps $d > 2$ is the statement that all points on the unstable manifold of the jth fixed point of F^n have the

same pointwise dimension which is given by (4.11) with the Lyapunov numbers λ_p replaced by the eigenvalues λ_{pj}.

The Hausdorff dimension $f(\alpha)$ of the set of points on the attractor with $D_p(\underline{x})=\alpha$ can also be obtained directly from this formulation. In particular, define $\hat{\Gamma}_\alpha$ to be the same as the expression in (4.6) with $q=0$ (for the Hausdorff dimension) and the sum restricted only to those fixed points j which satisfy $\alpha+\Delta\alpha \geq D_p(\underline{x}) \geq \alpha$,

$$\hat{\Gamma}_\alpha(D,\Delta\alpha,n)= \sum_{\alpha+\Delta\alpha \geq D_p(\underline{x}) \geq \alpha} \lambda_{2j}^{(D-1)} .$$

We then take limits,

$$\hat{\Gamma}_\alpha(D)= \lim_{\Delta\alpha\to 0} \lim_{n\to\infty} \hat{\Gamma}_\alpha(D,\Delta\alpha,n) ,$$

and we obtain $f(\alpha)$ as the transition value of D for which $\hat{\Gamma}_\alpha(D)$ goes from infinity to zero as D increases.

The results quoted in this section are for hyperbolic attractors (Sec. VI). For the two-dimensional hyperbolic case with $\lambda_{1j}>1>\lambda_{2j}$, we have $D_p(\underline{x})\geq 1$ for every point on the attractor. For the nonhyperbolic case, $D_p(\underline{x})$ can be less than 1, and we conjecture that (4.6) and (4.9) also hold in the nonhyperbolic case but only for q values corresponding to $\alpha(q)>1$ [cf. (3.11)].

Another result concerning ergodic properties of a map is that for the topological entropy S in terms of N_n, the number of fixed points of the n times iterated map $\underline{F}^n$,

$$S= \lim_{n\to\infty} \frac{1}{n} \log N_n . \tag{4.13}$$

For this result for the case of axiom A attractors see the papers by Bowen[6] and by Katok.[7]

V. EXAMPLES

We now illustrate the results on periodic orbits with two analytically tractable two-dimensional, hyperbolic map examples.

A. Example 1: The generalized baker's map

The generalized baker's map was introduced in Ref. 1 as a model for dimension studies which is amenable to analysis yet also has nonconstant stretching and contraction. We divide the square $0\leq(x,y)\leq 1$ into a bottom part, $0\leq y<a$, and a top part, $a<y\leq 1$. This is illustrated in Fig. 6(a) ($b=1-a$ in the figure). We compress the bottom (top) part by a factor λ_a (λ_b) along x, and stretch it in y by a factor a^{-1} (b^{-1}). We then have two rectangles, both of vertical height unity, one of width λ_a and the other of width λ_b [Fig. 6(b)]. We then move the λ_b width strip so that its lower left corner is at $x=\frac{1}{2}$, $y=0$ [Fig. 6(c)]. Thus we have a map of the unit square into itself: $x_{n+1}=\lambda(y_n)x_n+(\frac{1}{2})u(y_n-a)$; $y_{n+1}=\gamma(y_n)[y_n-\alpha u(y_n-a)]$; where $\lambda(y)=(\lambda_a,\lambda_b)$ for $y\gtrless a$, $\gamma(y)=(a^{-1},b^{-1})$ for $y\gtrless a$, and $u(y)$ is the unit step function.

Using similarity arguments[1] it can be shown directly from the map that the following transcendental equation determines D_q (cf. Refs. 2 and 3),

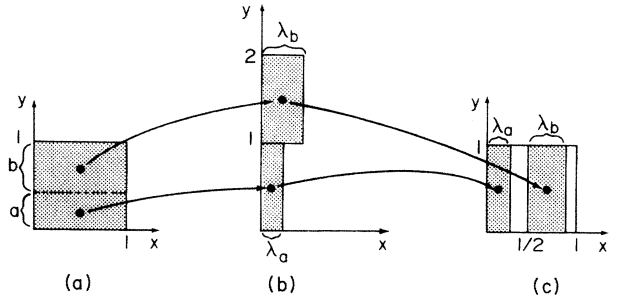

FIG. 6. Schematic of generalized baker's map.

$$1=\overline{A}+\overline{B} , \tag{5.1}$$

where $\overline{A}=\lambda_a^{-(q-1)(D_q-1)}a^q$, $\overline{B}=\lambda_b^{-(q-1)(D_q-1)}b^q$.

We now show that the equation determining the periodic point dimension $\hat{D}_q$ is the same as (5.1). We can specify an orbit for the generalized baker's transformation by its symbolic itinerary which specifies whether the orbit's location on successive iterates is in the top (symbolized by a 1) or in the bottom (symbolized by a 0). Thus a periodic orbit of period n which spends $k\leq n$ of its n iterates in $y>a$ is represented by a string of n symbols with k ones and $n-k$ zeros. The eigenvalues associated with such an orbit are $\lambda_2=\lambda_a^{n-k}\lambda_b^k$, $\lambda_1=a^{-(n-k)}b^{-k}$. Equation (4.6) yields

$$\hat{\Gamma}(q,D,n)= \sum_{k=0}^{n} N_{nk} A^{(n-k)}B^k , \tag{5.2}$$

where $A=a^q\lambda_a^{-(q-1)(D-1)}$, $B=b^q\lambda_b^{-(q-1)(D-1)}$, and N_{nk} is the number of fixed points of the n times iterated map which belong to periodic orbits which spend k iterates in the top ($y>a$). It can be shown that N_{nk} is the number of ways of arranging k zeros and $n-k$ ones,

$$N_{nk}=\binom{n}{k} . \tag{5.3}$$

Hence Eq. (5.2) is just a binomial expansion, $\hat{\Gamma}=(A+B)^n$. Letting $n\to\infty$, we see that the transition of $\hat{\Gamma}(q,D)$ from zero to infinity occurs at $D=D_q$ with D_q given by (5.1). Thus $D_q=\hat{D}_q$ for this example. [This calculation is algebraically equivalent to one in Halsey *et al.*,[4] although the basis for their calculation is Eq. (3.7), while the basis here is the periodic orbit formula, Eq. (4.6).]

To find $f(\alpha)$, we use (2.2) with λ_{1j} set equal to $a^{-(n-k)}b^{-k}$ and λ_{2j} set equal to $\lambda_a^{n-k}\lambda_b^k$ to obtain an equation relating α and $k/n\equiv\kappa$. This gives

$$\alpha=1+\frac{(1-\kappa)\log a+\kappa\log b}{(1-\kappa)\log\lambda_a+\kappa\log\lambda_b} .$$

Setting $q=0$ and using only the terms in the sum (5.2) with k/n values near that required by the specification of α and letting $n\to\infty$, we have (again using Stirling's approximation).

$$f(\alpha)=1+\frac{(1-\kappa)\log(1-\kappa)+\kappa\log\kappa}{(1-\kappa)\log\lambda_a+\kappa\log\lambda_b} , \tag{5.4}$$

with

$$\kappa=[\log a-(\alpha-1)\log\lambda_a]/[(\alpha-1)\log(\lambda_b/\lambda_a)+\log(a/b)] .$$

To obtain the topological entropy we note that $N_n=\sum_{k=0}^{n}N_{nk}$. Since N_{nk} is the binomial coefficient (5.3), this yields $N_n=2^n$, a well-known result for the baker's map. Equation (4.13) then gives $S=\log 2$, also well known.

It is also straightforward to verify Eq. (4.3). In particular, the right-hand side of (4.3) is $\sum\binom{n}{k}a^{n-k}b^k=(a+b)^n=1$ (recall $a+b=1$).

B. Example 2: The baker's apprentice's map

Example 1 has the property that setting $\hat{\Gamma}(q,D,n)=1$ gives precisely the desired result, Eq. (5.1), for all n, rather than only in the $n\to\infty$ limit. The generalized baker's map is exceptional in this regard, and this is due to the exact self-similarity of the attractor. A more typical example, which is still analytically tractable, is illustrated in Figs. 7. Again, we divide the unit square into top ($y>a$) and bottom ($y<a$) parts. We again horizontally compress the two parts by λ_a and λ_b. The bottom part is vertically stretched by a^{-1}, as before. The difference is that we now vertically compress the top part by a/b. The parts are then reassembled in the square as shown in Fig. 7(b). [We call this the baker's apprentice's map because the baker squashes and stretches the "dough" just right, so that it is exactly twice its original length, while the less experienced apprentice misses by not stretching enough to make the length double.]

Again we can specify orbits by a string of ones (tops) and zeros (bottoms). In this case, however, an orbit point in the top is always mapped to the bottom. Thus a one is *always* followed by a zero. Replacing B by $\tilde{B}=(b/a)^q\lambda_b^{-(q-1)(D-1)}$ (to account for the compression by a/b as opposed to the stretching by $1/b$ in example 1), we see that Eq. (5.2) still applies. Equation (5.3) for N_{nk}, however, does not.

To find N_{nk} we first note that the number of fixed points of the n times iterated map is the number of possible sequences of length n which contain k ones and $n-k$ zeros, subject to the constraint that a zero always follows a one (except when the last symbol is a one). We consider two cases: (a) the last symbol is a zero, and (b) the last symbol is a one. In case (a), to find the contribution to N_{nk} from such sequences, we regard the sequence (1,0) as a single symbol denoted by a 2. Thus a period n orbit which is located in the top k times is represented by a string of $(n-k)$ symbols of which k are twos and $n-2k$ are zeros (clearly $k\le n/2$). There are $\binom{n-k}{k}$ such symbol sequences. Sequences ending in the top [case (b)], on the other hand, end in a one. Since the sequence represents a periodic orbit it must also start with a zero. All the rest of the symbols can be thought of as zeros and twos. For this case the zero-two sequence has $n-k-1$ symbols of which $k-1$ are twos. There are $\binom{n-k-1}{k-1}$ sequences of this type. Thus we have

$$N_{nk}=\begin{bmatrix}n-k\\k\end{bmatrix}+\begin{bmatrix}n-k-1\\k-1\end{bmatrix}, \tag{5.5}$$

and $N_{nk}=0$ for $k>n/2$.

Using Stirling's approximation to expand $Z(\kappa)\equiv(1/n)\log(N_{nk}A^{(n-k)}\tilde{B}^k)$ for large n, we have

$$Z(\kappa)\cong(1-\kappa)\log(1-\kappa)-\kappa\log\kappa-(1-2\kappa)\log(1-2\kappa)+\kappa\log\tilde{B}+(1-\kappa)\log A\ , \tag{5.6}$$

where $\kappa=k/n$ and $\frac{1}{2}>\kappa>0$. The quantity Z is concave down ($d^2Z/d\kappa^2<0$) and has one maximum in $\frac{1}{2}>\kappa>0$. The location of this maximum is given by $\kappa_0(1-\kappa_0)=(1-2\kappa_0)^2\tilde{B}/A$. Since the summand in Eq. (5.2) is $\exp[nZ(\kappa)]$, if $n\to\infty$ and $Z(\kappa_0)<0$, then $\hat{\Gamma}(q,D)\to 0$. On the other hand, if $Z(\kappa_0)>0$, then $\hat{\Gamma}(q,D)\to\infty$. Thus at the transition we have the condition $Z(\kappa_0)=0$. This gives a transcendental equation for $\hat{D}_q$, $A+A\tilde{B}=1$, or

$$1=a^q\lambda_a^{(1-q)(\hat{D}_q-1)}+b^q(\lambda_a\lambda_b)^{(1-q)(\hat{D}_q-1)}\ . \tag{5.7}$$

We now show that D_q also satisfies Eq. (5.7). We employ the similarity technique[1-3] [used, for example, in Refs. 2 and 3 to obtain Eq. (5.1)]. We write the sum in the partition function, $\sum_i p_i^q/l_i^\tau$, as a sum over the top region plus a sum over the bottom region, $\Gamma(l)=\Gamma_T(l)+\Gamma_B(l)$. Similarly we write Γ_B as a sum over the bottom left ($x<\frac{1}{2}$), region plus a sum over the bottom right region,

$$\Gamma_B(l)=\Gamma_{BL}(l)+\Gamma_{BR}(l)\ . \tag{5.8}$$

Applying the map to one of the coverings of size l_i in the bottom, we see that it is compressed by λ_a and elongated by $1/\alpha$. Thus this l_i covering can be covered by $(a\lambda_a)^{-1}$ coverings of size $(l_i\lambda_a)$. Each of these new coverings has a probability $(p_i a\lambda_a)$. Inserting this information in the partition function Eq. (3.7) we have that

$$\Gamma_T(l\lambda_a)=\frac{b}{a\lambda_a}\left[\frac{(a\lambda_a)^q}{\lambda_a^\tau}\Gamma_B(l)\right]=\frac{b}{a}\frac{a^q}{\lambda_a^{(q-1)(D_q-1)}}\Gamma_B(l)\ .$$

Thus,

$$\Gamma_T(l)=\frac{b}{a}\frac{a^q}{\lambda_a^{(q-1)(D_q-1)}}\Gamma_B(l/\lambda_a)\ .$$

Similarly,

$$\Gamma_{BR}(l)=\frac{(b/a)^{q-1}}{\lambda_b^{(q-1)(D_q-1)}}\Gamma_T(l/\lambda_b)\ .$$

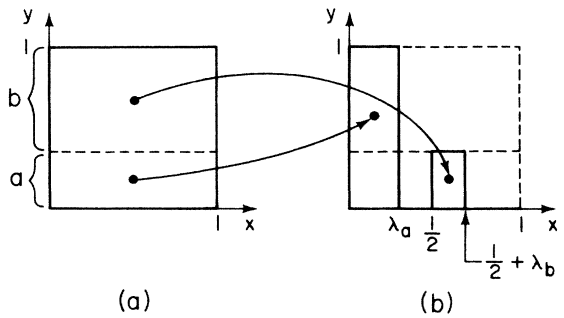

FIG. 7. Schematic illustrating the baker's apprentice's map.

Also, $\Gamma_{BL}=(a/b)\Gamma_T$. Combining these in (5.8) and letting $l\to 0$, we obtain (5.7), and hence $D_q=\hat{D}_q$ for this example as well.

To find $f(\alpha)$ for the apprentice's map, we again use $\alpha=D_p(\underline{x})$ with $D_p(\underline{x})$ given by (2.2). This gives

$$\alpha=1+\frac{(1-\kappa)\log a+\kappa\log(b/a)}{(1-\kappa)\log\lambda_a+\kappa\log\lambda_b} . \tag{5.9}$$

Including only values of k/n in the sum for $\hat{\Gamma}$ which nearly satisfies this relation and letting $n\to\infty$, we see that the Hausdorff dimension $f(\alpha)$ of the set where $\alpha=D_p(\underline{x})$ is given by setting $Z(\kappa)=0$ in Eq. (5.6) (with $q=0$),

$$f(\alpha)=1+\frac{(1-\kappa)\log(1-\kappa)-\kappa\log\kappa-(1-2\kappa)\log(1-2\kappa)}{(1-\kappa)\log\lambda_a+\kappa\log\lambda_b} \tag{5.10}$$

where from (5.9)

$$\kappa(\alpha)=\frac{\log a-(\alpha-1)\log\lambda_a}{(\alpha-1)\log(\lambda_b/\lambda_a)+\log(a^2/b)} .$$

To find the topological entropy we perform the sum

$$N_n=\sum_{k=0}^{n/2} N_{nk} ,$$

again by using Stirling's approximation. We obtain $N_n\sim G^n$, where $G=(1+\sqrt{5})/2$ is the golden mean. Thus from (4.13) the topological entropy is $S=\log G$.

Again one may verify Eq. (4.3) by direct calculation. The quantity to be obtained is

$$\lim_{n\to\infty}\sum_{k=0}^{n/2} N_{nk}(b/a)^k a^{n-k} .$$

The computation is somewhat tedious, but straightforward (use Stirling's approximation yet again), and yields 1, as it should.

To conclude this section, we emphasize that these two-dimensional map examples have both been shown to satisfy the conjectured equality of D_q with the periodic point dimension $\hat{D}_q$ [Eq. (4.9)].

VI. DEMONSTRATION OF THE RELATION OF UNSTABLE PERIODIC ORBITS TO THE ERGODIC PROPERTIES OF ATTRACTORS

In this section we obtain the results stated in Sec. IV and illustrated in Sec. V concerning the relationship of periodic orbits to ergodic properties of chaotic attractors. We shall do this only for the case of hyperbolic attractors which have a dense set of periodic orbits (i.e., axiom A attractors). Although our arguments are strictly only for the hyperbolic case, we believe that the results may be valid much more generally. For any point $\underline{x}$ in the phase space let $W^s(\underline{x})$ and $W^u(\underline{x})$ denote the stable and unstable manifolds of $\underline{x}$. The stable manifold of $\underline{x}$ is the set of points $\underline{y}$ such that $\|\underline{F}^n(\underline{x})-\underline{F}^n(\underline{y})\|\to 0$ as $n\to+\infty$ (Fig. 8); the unstable manifold is the set of points $\underline{z}$ such that $\|\underline{F}^{-n}(\underline{x})-\underline{F}^{-n}(\underline{z})\|\to 0$ as $n\to+\infty$ (we assume here that

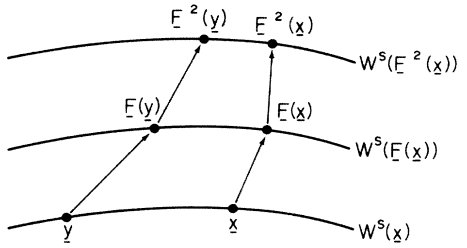

FIG. 8. Schematic illustrating the stable manifold of a point $\underline{x}$.

$\underline{F}$ is invertible). A hyperbolic attractor is one for which the following two conditions are satisfied.

(a) There exist stable and unstable manifolds $W^s(\underline{x})$ and $W^u(\underline{x})$ at each point $\underline{x}$ on the attractor that are not tangent and whose dimensions, d_s and d_u are the same for all $\underline{x}$ on the attractor, with $d_s+d_u=d$, where d is the dimension of the space. [Here $W^s(\underline{x})$ and $W^u(\underline{x})$ are smooth surfaces and d_s and d_u denote their Euclidean dimensions.]

(b) There exists a constant $K>1$ such that for all $\underline{x}$ on the attractor, if a vector $\underline{v}$ is chosen tangent to the unstable manifold, then

$$\|D\underline{F}(\underline{x})\underline{v}\|\geq K\|\underline{v}\| ,$$

and if $\underline{v}$ is chosen tangent to the stable manifold, then

$$\|D\underline{F}(\underline{x})\underline{v}\|\leq\|\underline{v}\|/K .$$

[Here $D\underline{F}(\underline{x})$ denotes the Jacobian matrix of partial derivatives of $\underline{F}(\underline{x})$ evaluated at $\underline{x}$.]

From condition (b) nearby points on the same stable (unstable) manifold approach (separate from) each other with time at least as fast as $\exp(-\kappa n)$ [$\exp(\kappa n)$]. For example, the magnitudes of the eigenvalues of $\underline{F}^n$ at a periodic point of a period n orbit must satisfy $\lambda_{pj}\geq K^n$ for $p\leq u$ and $\lambda_{pj}\leq K^{-n}$ for $p>u$. In particular, there can be no zero eigenvalues. In addition, it is very common for chaotic attractors encountered in practice to not be hyperbolic because they have points where $W^s(\underline{x})$ and $W^u(\underline{x})$ are tangent [in violation of condition (a)]. For example, the Henon attractor is of this type.

We first deal with two-dimensional maps (Secs. VI A–VI B) with $d_u=d_s=1$ and then indicate how the results can be extended to higher dimensions (Sec. VI C).

A. Measure

Imagine that we partition the space into cells C_i, where each cell has as its boundaries stable and unstable manifolds [Fig. 9(a)]. If the cells are very small, the curvature of the boundaries will be slight, and we can regard them as parallelograms [Fig. 9(b)]. Say we consider a given cell C_k and a large number of initial conditions sprinkled within the cell according to the natural probability measure on the attractor. Imagine that we iterate each of these initial conditions n times. After n iterates, a small fraction of the initial conditions may return to the small cell C_k. Since we assume the attractor to be ergodic and

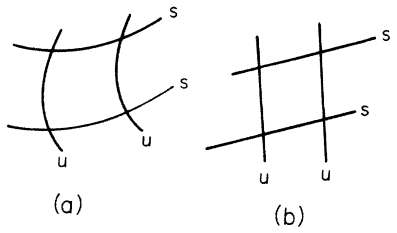

FIG. 9. Cells in a partition of the phase space. The letters s and u label stable and unstable manifold segments bounding the cell.

mixing this fraction is asymptotically (i.e., in the limit $n \to \infty$) equal to the natural measure of the attractor in the cell, $\mu(C_k)$. Let $\underline{x}_0$ be an initial condition that returns and $\underline{x}_n$ its nth iterate. This is illustrated in Fig. 10(a), where we take the stable direction as horizontal and the unstable direction as vertical. The line $ab(c'd')$ through $\underline{x}_0$ ($\underline{x}_n$) is a stable (unstable) manifold segment traversing the cell. Now take the nth forward iterate of ab and the nth backward iterate of $c'd'$. These map to $a'b'$ and cd as shown in Fig. 10(b). Now consider a rectangle constructed by passing unstable manifold segments $e'f'$ through a' and $g'h'$ through b'. By the construction, the nth preimages of these segments are the stable manifold segments ef and gh shown in Fig. 10(c). Thus we have constructed a rectangle $efgh$ in C_k such that all the points in $efgh$ return to C_k in n iterates. That is, $efgh$ maps to $e'f'g'h'$ in n iterates. The intersection of these two rectangles must contain a single saddle fixed point of the n times iterated map [cf. Fig. 10(d)]. Conversely, given a saddle fixed point, we can construct a rectangle of initial conditions $efgh$ which returns to C_k by closely following the periodic orbit which goes through the given fixed point j of $\underline{F}^n$ [the construction is the same as in Figs. 10(a)–10(c) except that $\underline{x}_0 = \underline{x}_n$]. Thus all initial conditions which return after n iterates lie in some long thin horizontal strip (like $efgh$) which contains a fixed point of the n times iterated map. We label this fixed point j and the magnitudes of its unstable and stable eigenvalues λ_{1j} and λ_{2j}. Denoting the horizontal and vertical lengths of the sides of the cell C_k by ξ_k and η_k [cf. Fig. 10(b)], we see that the initial strip $efgh$ has dimensions ξ_k by (η_k/λ_{1j}) and the final strip has dimensions $\xi_k\lambda_{2j}$ by η_k [cf. Fig. 10(d)]. Since the dynamics is expanding in the vertical direction, the attractor measure varies smoothly in this direction.[18] Since the cell is assumed small, we can treat the attractor as if it were essentially uniform along the vertical direction. Thus the fraction of the measure of C_k occupied by the strip $efgh$ is $1/\lambda_{1j}$. Since, for $n \to \infty$, the fraction of initial conditions starting in C_k which return to it is $\mu(C_k)$, we have

$$\mu(C_k) = \lim_{n\to\infty} \left[\sum_{\substack{\text{fixed points} \\ \text{in } C_k}} \lambda_{1j}^{-1} \right] . \tag{6.1}$$

(Also note that, as n gets larger, λ_{1j}^{-1} and λ_{2j} get exponentially smaller and the number of fixed points in C_k grows exponentially.) Since we imagine that we can make the partition into cells as small as we wish, we can approximate any subset S of the phase space (with reasonably smooth boundaries) by a covering of cells. Thus we obtain the result, Eq. (4.2), of Sec. IV (with $L_j = \lambda_{1j}$ for the case treated here; i.e., $d = 2$ with saddle periodic orbits).

In the construction which we used in arriving at Eq. (6.1), we have made two implicit assumptions. Namely, we have assumed that the segment ab maps to a segment $a'b'$ which lies entirely within C_k [i.e., we assume that the situation in Fig. 11(a) does not occur], and we have assumed that the preimage of $c'd'$ is entirely within C_k [i.e., Fig. 11(b) does not occur]. These situations might conceivably occur if $\underline{x}_n$ is too close ($\sim \xi_k\lambda_{2j}$) to a stable boundary or if $\underline{x}_0$ is too close ($\sim \eta_k/\lambda_{1j}$) to an unstable boundary. The point we wish to make here is that, for hyperbolic systems, the partition into cells can be chosen in such a way that the situations depicted in Fig. 11 do not occur. Such partitions are called Markov partitions.[18]

A Markov partition[18] satisfies the following condition. Say we have a Markov partition into cells C_i. Then, if $\underline{x}$ is in cell C_k and $\underline{F}(\underline{x})$ is in cell C_l, we have that

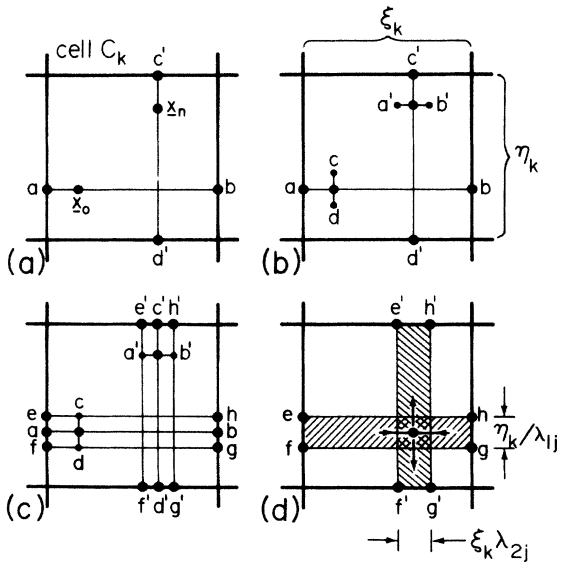

FIG. 10. Schematic of the construction of a rectangle in cell C_k which returns to C_k.

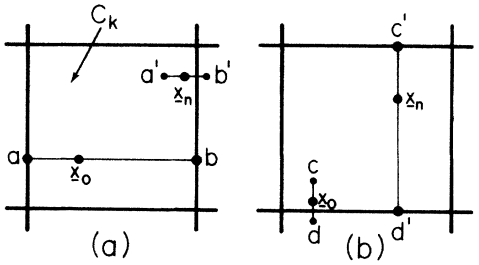

FIG. 11. Schematic depicting what can happen if $\underline{x}_0$ or $\underline{x}_n$ is too close to the boundary of C_k and a Markov partition is not used.

$$\underline{F}(W^u(\underline{x},C_k))\supset W^u(\underline{F}(\underline{x}),C_l)\ , \tag{6.2a}$$

$$\underline{F}(W^s(\underline{x},C_k))\subset W^s(\underline{F}(\underline{x}),C_l)\ , \tag{6.2b}$$

where $W^u(\underline{x},C_k)$ denotes a segment of the unstable manifold of $\underline{x}$ which traverses C_k passing through $\underline{x}$, and similarly for $W^s(\underline{x},C_k)$. Equations (6.2) are illustrated in Fig. 12. [Note that, to satisfy (6.2a), the end points of $\underline{F}(W^u(\underline{x},C_k))$ map to cell boundaries.] As an example, Fig. 13 shows a succession of finer Markov partitions for the baker's apprentice's map. The unit square, Fig. 13(a), is mapped into itself and bounded by segments of stable (horizontal) and unstable (vertical) manifolds. The boundaries of the partitions are obtained by taking forward iterates of the vertical (unstable) boundaries and backward iterates of the horizontal (stable) boundaries (as is explained further in the caption to Fig. 13).

Remark. The arguments as presented are not rigorous, but can be made rigorous. In particular, our arguments assume that we can approximate the map on each cell C_k as if it were linear. Also we assume that n is very large, giving the mixing sufficient time to make the probability of returning to C_k nearly equal to the measure $\mu(C_k)$. Detailed calculations based on the second derivative of the map show that our linear estimate (6.1) can be in error by at most a factor of $1\pm\epsilon$, where ϵ depends on the size of C_k and the size of the second-order partial derivatives of the map. Since we can make the size of C_k uniformly small, we can make ϵ uniformly small. Hence Eq. (4.2) holds exactly.

B. Dimension

In Fig. 10 the attractor measure contained in $e'f'g'h'$ is $1/\lambda_{1j}$. Say we cover $e'f'g'h'$ with boxes of edge length ξ_k/λ_{2j} corresponding to the narrow width of $e'f'g'h'$. There are $m_j=\eta_k/(\xi_k\lambda_{2j})$ such boxes. Since the attractor measure in the cell is essentially uniform along the vertical direction, the measure contained within one of the small boxes of edge length $\xi_k\lambda_{2j}$ is $1/(\lambda_{1j}m_j)$. Thus the contribution from $e'f'h'g'$ to the sum $\sum_i p_i^q/l_i^\tau$ in Eq. (3.7) is $m_j(\lambda_{1j}m_j)^{-q}(\xi_k\lambda_{2j})^{-\tau}$, or

$$\chi_k\frac{1}{\lambda_{1j}^q\lambda_{2j}^{(q-1)(D-1)}}\ ,$$

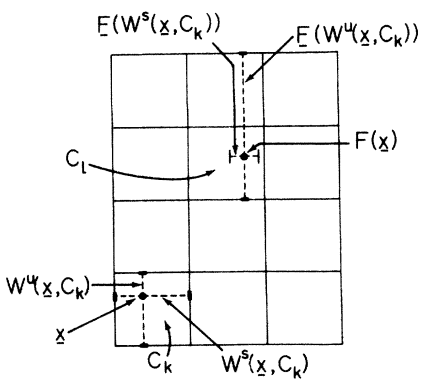

FIG. 12. Schematic illustrating Eqs. (6.2).

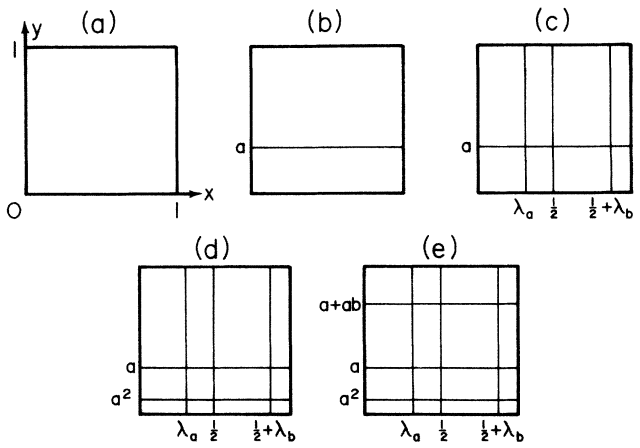

FIG. 13. Several successively finer Markov partitions for the baker's apprentice's map. Starting with (a), (b) is obtained by taking a preimage of the horizontal line $y=1$ (which is a stable manifold segment). (c) is obtained by taking a forward iterate of the vertical (unstable manifold) segments, $x=0$ and $x=1$. (d) is obtained by taking a preiterate of $y=a$ in (b), and (e) is obtained from (d) by preiterating $y=a^2$, etc.

where

$$\chi_k=(\eta_k\xi_k^{D-1})^{-(q-1)}\ .$$

Note that χ_k depends only on the partition and not on n. For a given partition there will be some cell $k=k_M$ where χ_k is the largest and some cell $k=k_m$ where χ_k is the smallest

$$\chi_{k_M}\geq\chi_k\geq\chi_{k_m}\ . \tag{6.3}$$

Now summing over all boxes we have

$$\sum_i p_i^q/l_i^\tau=\sum_j\chi_k\frac{1}{\lambda_{1j}^q\lambda_{2j}^{(q-1)(D-1)}}\ . \tag{6.4}$$

Using the bound (6.3), we have for the quantity in (6.4)

$$\chi_{k_M}\hat{\Gamma}(q,D,n)\geq\sum_j\chi_k\frac{1}{\lambda_{1j}^q\lambda_{2j}^{(q-1)(D-1)}}\geq\chi_{k_m}\hat{\Gamma}(q,D,n)\ , \tag{6.5}$$

where $\hat{\Gamma}(q,D,n)$ is given by (4.6). Letting $l\to0$ in (3.9) is analogous to letting $n\to\infty$, since the box edge length used for the cover of $e'f'g'h'$ is edge $\xi_k\lambda_{2j}$, and λ_{2j} decreases exponentially with n. Letting n go to infinity, we see that the right-hand side of (6.4) goes through a transition from zero to infinity at the same value of D (denoted $\hat{D}_q$) as does $\sum_i p_i^q/l_i^\tau$. Furthermore, by (6.5) this transition also occurs at $D=\hat{D}_q$ for $\hat{\Gamma}(q,D)$ given by (4.6). This is the desired result for the two-dimensional map case.

In the above we have used a particular covering in obtaining the result (6.4) for $\sum_i p_i^q/l_i^\tau$. In particular, we have used the covering suggested by the dynamics and the Markov partition [cf. Fig. 10(d)]. However, since we have not optimized over all coverings, $\hat{D}_q$ the transition value of $\lim_{l\to0}\sum_i p_i^q/l_i^\tau$ might overestimate D_q. That is

$\hat{D}_q$ is an upper bound to D_q, Eq. (4.8). It appears, however, that the covering of the attractor that we use is a rather efficient one, and we therefore believe that $D_q = \hat{D}_q$ for typical chaotic attractors. This is confirmed for the examples in Sec. V. [Furthermore, note that our result has turned out to be independent of the particular choice of the Markov partition (i.e., $\hat{\Gamma}$ does not involves χ_k).]

C. Systems of higher dimension

Again we consider a Markov partition, this time in a d-dimensional ($d > 2$) space. A fixed point j in a small cell C_k has associated with it a d-dimensional parallelepiped of initial conditions extending across the cell in the stable directions and thin in the unstable directions. The nth iterate of this parallelepiped is a d-dimensional "slab" which extends across the cell in the unstable directions and is thin in the stable directions. This is illustrated for the case $d = 3$ and $\lambda_{1j} > \lambda_{2j} > 1 > \lambda_{3j}$ (i.e., two unstable and one stable direction) in Fig. 14. Using this construction, it is readily seen that the derivation given in Sec. VI A for Eq. (6.1) extends to the higher dimensional case, for which we obtain Eq. (4.2). Now we turn to a consideration of the partition function for $d > 2$. As shown in Eqs. (6.3)–(6.5) of Sec. VI B, the dimensions of the cells do not affect the final result; thus, for simplicity we set the d edge lengths of the cell C_k equal to 1 (e.g., $\xi_k = \eta_k = \beta_k = 1$ in Fig. 14). Now we cover the slab (cf. Fig. 14) with small d-dimensional cubes. We choose the edge length of the small cubes to be $\lambda_{(k+1)j}$, where we leave k unspecified for the moment, except to say that k is large enough so that $\lambda_{(k+1)j} < 1$ (or $k \geq u$ where u denotes the number of unstable eigenvalues). The number of such small cubes necessary to cover the slab is

$$m_j = \frac{\lambda_{1j}\lambda_{2j}\cdots\lambda_{kj}}{(\lambda_{(k+1)j})^k}\frac{1}{L_j} .$$

The probability measure of the attractor in the slab is L_j^{-1}. Thus, if the measures in each cube used to cover the slab are equal, then

$$p_i = \frac{1}{m_j L_j} \equiv \bar{p} . \tag{6.6}$$

The assumption of equal probabilities was justified in the two-dimensional case (Sec. VI B) by the fact that the measure varies smoothly along unstable manifolds. In the case considered here, however, k can be greater than u. The directions corresponding to subscripts $u+1, u+2, \ldots, k$ are not stretching. Thus the assumption of equal probabilities is not as well founded as it was in Sec. VI B. Nevertheless, it is still useful, as we now show. The contribution to $\sum_i p_i^q / l_i^\tau$ from the slab is $\lambda_{(k+1)j}^{-\tau} \sum_{\text{slab}} p_i^q$. The sum $\sum_{\text{slab}} p_i^q$ subject to the constraint $\sum_{\text{slab}} p_i = L_j^{-1}$ is bounded by the value it assumes when all of the p_i in the slab are equal,

$$\sum_{\text{slab}} p_i^q \leq m_j \bar{p}^{\,q} \quad \text{for} \quad q < 1 ,$$

$$\sum_{\text{slab}} p_i^q \geq m_j \bar{p}^{\,q} \quad \text{for} \quad q > 1 .$$

Thus using (6.6) for $q < 1$ can only increase $\hat{\Gamma}(q,D)$. From Fig. 5(b) we see that this can possibly increase the transition value of D but not decrease it. Similarly, using (6.6) for $q > 1$ can only decrease $\hat{\Gamma}(q,D)$, again leading to a possible increase in the transition value of D [cf. Fig. 5(c)]. Thus, we conclude that using (6.6) to obtain $\hat{\Gamma}$ will give a transition value of D for $\hat{\Gamma}$ which is an upper bound on D_q [Eq. (4.8)]. Using (6.6) the contribution to $\sum_i p_i^q / l_i^\tau$ from the slab is

$$m_j \left[\frac{1}{m_j L_j}\right]^q \frac{1}{(\lambda_{(k+1)j})^{(q-1)D}} = L_j^{-1}[S_{kj}(D)]^{-(q-1)} ,$$

where

$$S_{kj}(D) = m_j L_j (\lambda_{(k+1)j})^D = \lambda_{1j}\lambda_{2j}\cdots\lambda_{kj}(\lambda_{(k+1)j})^{(D-k)} .$$

In accord with the supremum for $q > 1$ and the infimum for $q < 1$ in Eq. (3.8), we choose k to make $S_{kj}(D)$ as small as possible. Increasing k decreases $S_{kj}(D)$ so long as $D - k > 0$ (recall that $\lambda_{(k+1)j} < 1$). Thus $k = \Delta$, where Δ is the integer part of D, and the minimum $S_{kj}(D)$ is $S_j(D)$ given in Eq. (4.4). Now summing over all fixed points and all cells, we obtain the desired result, Eq. (4.5). We note that due to the possible nonuniformity of p_i within the slabs, our conjecture (4.9) is not on as firm ground for $d > 2$ as it is for the case $d = 2$ treated in Sec. VI B.

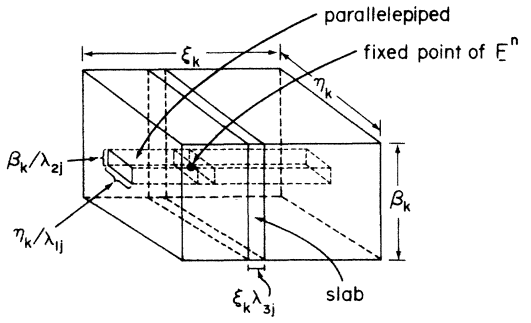

FIG. 14. Schematic illustrating a cell in the partition for $d = 3$ with two unstable and one stable direction.

VII. TRANSIENT CHAOS

In many situations there are sets with chaotic dynamics which are not attractors. While such sets do not lead to long-term chaotic behavior of typical initial conditions, they do have an important effect on the gross dynamics.[10,19–21] In particular, they manifest themselves by the presence of chaotic transients. It is the purpose of this section to extend some of the results of the previous section to the case of chaotic sets which are not attracting.

Imagine a region of space Λ which encloses what we shall call a strange saddle. This is illustrated for $d = 2$ in Fig. 15. This figure shows the saddle as the intersection of its stable and unstable manifolds, both of which may

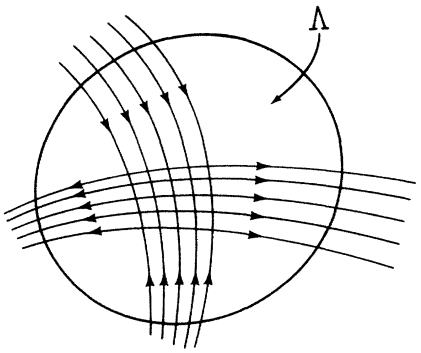

FIG. 15. Strange saddle and its stable and unstable mani folds, and a region Λ containing the strange saddle.

be thought of as a Cantor set of roughly parallel lines. If we sprinkle N_0 initial conditions uniformly in Λ, on subsequent iterates, the orbits leave Λ never to return. Let N_n be the number of orbits that have not left Λ after n iterates. For large n this number will decay exponentially with time,

$$(N_n/N_0)\sim\exp-(n/\tau) , \tag{7.1}$$

where we call τ the lifetime of the chaotic transient. We can define a natural measure for this process as follows. Let W be a subset of Λ. The natural measure of W is

$$\mu(W)=\lim_{n\to\infty}\lim_{N_0\to\infty} N_n(W)/N_n , \tag{7.2}$$

where $N_n(W)$ is the number of orbit points which fall in W at time n. Equations (7.1) and (7.2) imply that if initial conditions are distributed in accord with the natural measure and evolved in time, then the distribution will decay exponentially at the rate $1/\tau$. (This is not an invariant measure.) Points which leave Λ after a long time do so by being attracted along the stable manifold of the saddle, bouncing around on the saddle in a, perhaps, chaotic way, and then exiting along the unstable manifold.[10,19] The natural measure (7.2) is thus concentrated along the unstable manifold of the strange saddle.

Proceeding as in Sec. VI A, one can show that [compare with (4.3)]

$$\lim_{n\to\infty} e^{n/\tau}\sum_j L_j^{-1}=1 , \tag{7.3}$$

from which the transient lifetime can be determined,

$$\frac{1}{\tau}=\lim_{n\to\infty}\left[\frac{1}{n}\log\left[\sum_j L_j^{-1}\right]^{-1}\right] . \tag{7.4}$$

This equation has been previously conjectured in Ref. 8 where numerical experiments verifying it are also reported. The quantity on the right-hand side of Eq. (7.4) is called the pressure and plays an important role in the ergodic theory of dynamical systems.

One can also ask what the dimensions D_q and $f(\alpha)$ are for the natural measure,[20,21] Eq. (7.2). Proceeding as in Secs. VI B and VI C, we find that the relevant partition function is

$$\hat{\Gamma}(q,D,n)=e^{qn/\tau}\sum_j \frac{1}{L_j}[S_j(D)]^{-(q-1)} . \tag{7.5}$$

In (7.5) the sum is over all fixed points of $\underline{F}^n$ which lie on the strange saddle. [The factors $e^{n/\tau}$ and $e^{qn/\tau}$ that appear in Eqs. (7.3) and (7.5) do so essentially in order to compensate for the exponential time decay of orbits in Λ which start with initial conditions distributed in accord with the natural measure (7.2).]

Formally expanding Eq. (7.5) in powers of $q-1$ [as was done in Sec. IV to obtain Eq. (4.10)], we find that the information dimension of the natural measure is

$$D_1=\Delta+\frac{\log(\bar{\lambda}_1\bar{\lambda}_2\cdots\bar{\lambda}_\Delta)-1/\tau}{\log(1/\bar{\lambda}_{\Delta+1})} , \tag{7.6}$$

where the Lyapunov numbers $\bar{\lambda}_p$ in this equation are defined in terms of the periodic orbits as follows:

$$\log\bar{\lambda}_p=\lim_{n\to\infty}\frac{e^{n/\tau}}{n}\sum_j\frac{1}{L_j}\log\lambda_{pj} . \tag{7.7}$$

Equation (7.6) has been given in Ref. 20 for the two-dimensional case, with the Lyapunov numbers defined in terms of typical orbits rather than periodic orbits [Eq. (7.7)], and we conjecture that the two definitions yield the same Lyapunov numbers. Note that for attractors $\tau\to\infty$ and (7.6) recovers the Kaplan-Yorke formula, Eq. (4.11).

VIII. CONCLUSION

The main result of this paper is a partition function formalism for determining the spectrum of fractal dimensions in terms of unstable periodic orbits. Beyond its conceptual appeal and potential use in further theoretical developments, the utility of this formalism will depend on how easy or difficult it is to extract information on periodic orbits from numerical computations and experimental data.[8–10]

ACKNOWLEDGMENTS

This work was supported by the U.S. Department of Energy (Basic Energy Sciences) and by the U.S. Office of Naval Research.

APPENDIX: NATURAL MEASURE

At the beginning of Sec. II we have given a definition of the natural measure which is adequate for "most purposes." A difficulty with the definition as stated can occur in special cases. For example, if the attractor has zero phase-space volume and we let the set S be the attractor itself, then, for almost every $\underline{x}$ in the basin of attraction, $\mu(\underline{x},S)$ as defined is zero (for finite length trajectories, the orbit approaches S but is not on S). A proper definition should give $\mu(S)=1$ for this S. To correct this, one can define $\mu(\underline{x},S)$ in a slightly different way. Let $\mu_\epsilon(\underline{x},S)$ be the fraction of time the trajectory originating at $\underline{x}$ spends in the ϵ neighborhood of S, and define

$$\mu(\underline{x},S)=\lim_{\epsilon\to0^+}\mu_\epsilon(\underline{x},S) .$$

If this $\mu(\underline{x},S)$ is the same for almost every $\underline{x}$ in the attractor basin, then we denote this value $\mu(S)$ and call it the natural measure of the attractor.

[1]J. D. Farmer, E. Ott, and J. A. Yorke, Physica D **7**, 153 (1983).
[2]P. Grassberger, Phys. Lett. **97A**, 227 (1983).
[3]H. G. E. Hentschel and I. Procaccia, Physica D **8**, 435 (1983).
[4]P. Grassberger, Phys. Lett. **107A**, 101 (1985); T. C. Halsey, M. J. Jensen, L. P. Kadanoff, I. Procaccia, and B. I. Shraiman, Phys. Rev. A **33**, 1141 (1986).
[5]C. Grebogi, E. Ott, and J. A. Yorke, Phys. Rev. A **36**, 3522 (1987). Recent related works are the following: T. Morita, H. Hata, H. Mori, T. Horita, nd K. Tomita, Progr. Theor. Phys. **78**, 511 (1987); G. Gunaratne and I. Procaccia, Phys. Rev. Lett. **59**, 1377 (1987); M. H. Jensen (unpublished).
[6]R. Bowen, Trans. Am. Math. Soc. **154**, 377 (1971).
[7]A. B. Katok, Publ. Math. IHES **51**, 137 (1980).
[8]L. P. Kadanoff and C. Tang, Proc. Natl. Acad. Sci. USA **81**, 1276 (1984).
[9]D. Auerbach, P. Cvitanovic, J.-P. Eckmann, G. Gunaratne, and I. Procaccia, Phys. Rev. Lett. **58**, 2387 (1987).
[10]C. Grebogi, E. Ott, and J. A. Yorke, Phys. Rev. Lett. **57**, 1284 (1986); Phys. Rev. A **36**, 5365 (1987).
[11]M. V. Berry, in *Chaotic Behavior of Deterministic Systems,* edited by G. Iooss, R. H. G. Helleman, and R. Stora (North-Holland, Amsterdam, 1983), p. 171–271.
[12]J. H. Hannay and A. M. Ozorio de Almeida, J. Phys. A **17**, 3429 (1984).
[13]M. V. Berry, Proc. R. Soc. London A **400**, 229 (1985).
[14]F. Hausdorff, Math. Annalen **79**, 157 (1918).
[15]A. N. Kolmogorov, Dokl. Akad. Nauk SSSR **119**, 861 (1958).
[16]A. Renyi, Acta Mathematica (Hungary) **10**, 193 (1959).
[17]J. Kaplan and J. Yorke, in *Functional Differential Equations and the Approximation of Fixed Points,* Vol. 730 of *Lecture Notes in Mathematics,* edited by H. O. Peitgen and H. O. Walther (Springer, Berlin, 1978), p. 228.
[18]R. Bowen, *On Axiom A Diffeomorphisms,* CBMS Regional Conference Series in Mathematics (American Mathematical Society, Providence, 1978), Vol. 35.
[19]C. Grebogi, E. Ott, and J. A. Yorke, Physica D **7**, 181 (1983).
[20]H. Kantz and P. Grassberger, Physica D **17**, 75 (1985); G. Hsu, E. Ott, and C. Grebogi, Phys. Lett. A (to be published).
[21]P. Szépfalusy and T. Tél, Phys. Rev. A **34**, 2520 (1986).

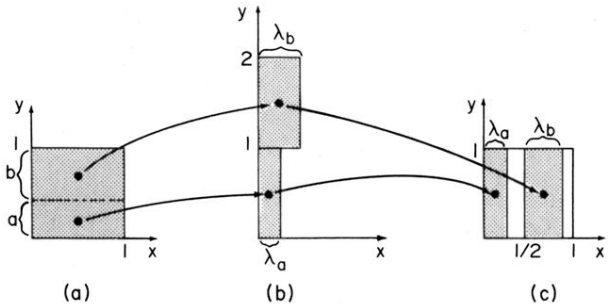

FIG. 6. Schematic of generalized baker's map.